

# 2-D Euler Shape Design on Nonregular Flows Using Adjoint Rankine–Hugoniot Relations

Antonio Baeza\*

Madrid Institute for Advanced Studies in Mathematics, 28049 Madrid, Spain

Carlos Castro†

Universidad Politécnica de Madrid, 28040 Madrid, Spain

Francisco Palacios‡

Madrid Institute for Advanced Studies in Mathematics, 28049 Madrid, Spain

and

Enrique Zuazua§

Basque Center for Applied Mathematics, 48009 Bilbao, Spain

DOI: 10.2514/1.37149

Optimal aerodynamic shape design aims to find the minimum of a functional that describes an aerodynamic property, by controlling the partial differential equation modeling the dynamics of the flow that surrounds an aircraft, by using surface deformation techniques. As a solution to the enormous computational resources required for classical shape optimization of functionals of aerodynamic interest, probably the best strategy is to apply methods inspired in control theory. One of the key ingredients relies on the usage of the adjoint methodology to simplify the computation of gradients. In this paper we restrict our attention to optimal shape design in two-dimensional systems governed by the steady Euler equations for flows whose steady-state solutions present discontinuities in the flow variables (an isolated shock wave). We first review some facts on control theory applied to optimal shape design and recall the 2-D Euler equations (including the Rankine–Hugoniot conditions). We then study the adjoint formulation, providing a detailed exposition of how the derivatives of functionals of aeronautical interest may be obtained when a discontinuity appears. Further on, adjoint equations will be discretized and analyzed and some novel numerical experiments with adjoint Rankine–Hugoniot relations will be shown. Finally, we expose some conclusions about the viability of a rigorous approach to the continuous Euler adjoint system with discontinuities in the flow variables.

## Nomenclature

$\mathbf{A}$	= Jacobian matrix for the convective fluxes
$C_D$	= drag coefficient
$C_L$	= lift coefficient
$C_p$	= pressure coefficient
$c$	= local speed of sound
$E$	= total energy
$\mathbf{F}$	= vector of convective fluxes
$\mathbf{f}$	= vector of numerical fluxes
$H$	= enthalpy
$J$	= cost function
$\mathbf{n}$	= normal vector
$P$	= static pressure
$S$	= solid wall boundary
$\mathcal{S}_{\text{ad}}$	= space of admissible surfaces
$s$	= speed of shock wave propagation
$\mathbf{t}$	= unit tangent vector
$\mathbf{U}$	= vector of conserved variables
$\mathbf{v}$	= velocity vector
$\mathbf{W}$	= vector of characteristic variables

Presented as Paper 171 at the 46th AIAA Aerospace Sciences Meeting and Exhibit, Reno, Nevada, 7–10 January 2008; received 14 February 2008; revision received 29 September 2008; accepted for publication 9 November 2008. Copyright © 2008 by the American Institute of Aeronautics and Astronautics, Inc. All rights reserved. Copies of this paper may be made for personal or internal use, on condition that the copier pay the \$10.00 per-copy fee to the Copyright Clearance Center, Inc., 222 Rosewood Drive, Danvers, MA 01923; include the code 0001-1452/09 \$10.00 in correspondence with the CCC.

\*Researcher, iMath Project FUT-C2-0038.

†Assistant Professor, Departamento de Matemáticas e Informática, ETSI Caminos, Canales y Puertos.

‡Director of Technological Innovation, IMDEA-Mathematics. Member AIAA.

§Scientific Director, Basque Center for Applied Mathematics (BCAM).

$\mathbf{x}$	= Cartesian coordinates vector
$x_b$	= intersection between a shock wave and a solid surface
$\alpha$	= angle of attack
$\Gamma_\infty$	= “far-field” boundary
$\gamma$	= ratio of specific heat
$\Delta$	= first difference
$\delta$	= first variation
$\partial$	= partial derivative
$\partial_n$	= normal derivative to a curve
$\partial_{tg}$	= tangent derivative to a curve
$\eta$	= curve parameter
$\kappa$	= curvature of a curve
$\Lambda$	= diagonal matrix of inviscid eigenvalues
$\rho$	= density
$\Sigma$	= shock wave curve
$\Psi$	= vector of adjoint variables
$\Omega$	= fluid domain

## I. Introduction

IN THE last decades, optimal shape design in aeronautics has evolved very close to the computational fluid dynamics developments. By the 1980s, advances in computer hardware and algorithms made it feasible to develop accurate and efficient analysis tools for inviscid flows [1]. On the other hand, control theory was significantly developed with, in particular, the groundbreaking works due to Lions [2]. Several years later, Pironneau investigated the problem of optimum shape design for elliptic equations using control theory [3]. In the late 1980s, Jameson [4] was the first to apply these techniques to the Euler and Navier–Stokes equations in the field of aeronautical applications. At the beginning of the twenty-first century, new techniques such as the reduced gradient formulation [5] and the systematic approach [6] made a significant simplification to the continuous adjoint implementation on unstructured meshes.

The goal of optimal shape design is to minimize a suitable cost or objective function (drag coefficient, deviation from a prescribed surface pressure distribution, etc.) with respect to a set of design variables (defining, for example, an airfoil profile or aircraft surface). Widely used methods are based on gradient descent techniques, where minimization is achieved by means of an iterative process, which requires the computation of the gradients or sensitivity derivatives of the cost function with respect to the design variables.

If the flow is assumed to be smooth, the perturbation of the flowfield variables with respect to shape changes can be calculated by linearizing the governing equations (or using a more elaborate technique such as the adjoint state). However, this is not valid in the neighborhood of flow discontinuities. Several options have been proposed in the literature to deal with nonsmooth flows, in particular, by Iollo et al. [7], Giles and Pierce [8], Matsuzawa and Hafez [9], Cliff et al. [10], and Castro et al. [11]. Currently, most existing works ignore the shock motion sensitivity supposing that shocks are smeared using numerical dissipation. However, this paper is intended to clarify that appropriate treatment of shock waves is important in some situations and leads to the computation of more accurate gradients that lead to faster optimization loops.

Aerodynamic applications of optimal shape design [12] in systems governed by partial differential equations are formulated on a fluid domain  $\Omega$ , containing a compressible fluid, usually air, delimited by disconnected boundaries divided into a “far field”  $\Gamma_\infty$  and one or more solid wall boundaries  $S$ , usually airplane surfaces (see Fig. 1).

From now on we will restrict ourselves to the analysis of optimization problems involving functionals  $J$  defined on the solid wall  $S$ , whose value depends on the flow variables  $U$  obtained from the solution of the fluid flow equations. In this context, the generic optimization problem can be succinctly stated as follows: find  $S^{\min} \in \mathcal{S}_{\text{ad}}$  such that

$$J(S^{\min}) = \min_{S \in \mathcal{S}_{\text{ad}}} J(S) \quad (1)$$

where  $\mathcal{S}_{\text{ad}}$  is the set of admissible boundary geometries and

$$J(S) = \int_S j(P, \mathbf{n}_S) \, ds \quad (2)$$

is the objective function, where  $j(P, \mathbf{n}_S)$  is a smooth function which depends on  $\mathbf{n}_S$  (inward-pointing unit vector normal to  $S$ ) and the pressure  $P$ . The evaluation of  $J(S)$  requires the resolution of the flow equations to obtain  $P$ .

It is worth mentioning that only functionals which depend on the pressure  $P$  alone are allowed a priori [6,13]. Luckily, functionals which depend solely on the pressure are the most common in aerodynamic design applications with Euler equations (e.g., lift or drag coefficients).

Let us consider a small perturbation of the boundary  $S$  which, without loss of generality, can be parameterized by a deformation of size  $\delta S$  along  $\mathbf{n}_S$ . The deformed surface can be written as

$$S' = \{\mathbf{x} + \delta S(\mathbf{x})\mathbf{n}_S(\mathbf{x}), \mathbf{x} \in S\} \quad (3)$$

Assuming a regular flow solution, the variation of the functional  $J$  under the deformation can be evaluated as [11,14]

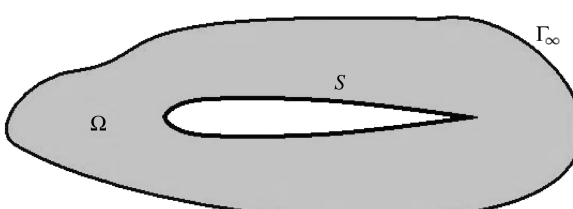


Fig. 1 Classical optimal design problem.

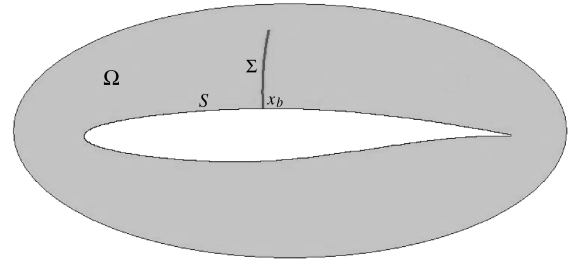


Fig. 2 Optimal design problem with a shock wave  $\Sigma$ .

$$\begin{aligned} \delta J(S) = & \int_S \left[ \frac{\partial j}{\partial P} \partial_n P + \mathbf{t} \cdot \partial_{tg} \left( \frac{\partial j}{\partial \mathbf{n}_S} \right) - \kappa \left( j + \frac{\partial j}{\partial \mathbf{n}_S} \mathbf{n}_S \right) \right] \delta S \, ds \\ & + \int_S \frac{\partial j}{\partial P} \delta P \, ds \end{aligned} \quad (4)$$

where  $\kappa$  is the curvature<sup>¶</sup> of  $S$ , and  $\delta P$  stands for the infinitesimal variation of the pressure. The first term on the right-hand side (RHS) of Eq. (4) stems from the displacement of the boundary and the last term is the contribution due to infinitesimal changes in the flow solution induced by the deformation.

On the other hand, nonregular solutions of the flow variables are the most common case in aeronautical applications and appear in transonic and supersonic flow regimes. Transonic inviscid flows are characterized by the appearance of shock waves that extend from the flowfield to the surface of the body. In these cases a discontinuity (shock wave) along a regular curve  $\Sigma$  must be considered (see Fig. 2) and the Rankine–Hugoniot relations must be added to the Euler equations to correctly account for the presence of the shock.

If the flow presents a discontinuity that touches the surface  $S$  then the previous computation of the derivative of the functional in Eq. (4) fails and has to be modified to include the effect due to the sensitivity of the shock location with respect to shape deformations [15].

Let  $x_b = \Sigma \cap S$  that we assume to be a unique point. Then the expression for  $\delta J$  is

$$\begin{aligned} \delta J(S) = & \int_{S \setminus x_b} \left[ \frac{\partial j}{\partial P} \partial_n P + \mathbf{t} \cdot \partial_{tg} \left( \frac{\partial j}{\partial \mathbf{n}_S} \right) - \kappa \left( j + \frac{\partial j}{\partial \mathbf{n}_S} \mathbf{n}_S \right) \right] \delta S \, ds \\ & + \int_{S \setminus x_b} \frac{\partial j}{\partial P} \delta P \, ds - \frac{[j]_{x_b}}{\mathbf{n}_S \cdot \mathbf{t}_\Sigma} (\delta \Sigma(x_b) - (\mathbf{n}_S \cdot \mathbf{n}_\Sigma) \delta S(x_b)) \\ & - \mathbf{t} \cdot \left[ \frac{\partial j}{\partial \mathbf{n}_S} \right]_{x_b} \delta S(x_b) \end{aligned} \quad (5)$$

where, to define  $\mathbf{n}_\Sigma = (n_{\Sigma_x}, n_{\Sigma_y})$ , we first consider  $\mathbf{t}_\Sigma = (t_{\Sigma_x}, t_{\Sigma_y})$ , the unitary tangent vector to the discontinuity beginning at the solid surface and pointing to the far-field boundary, and then set  $\mathbf{n}_\Sigma = (n_{\Sigma_x}, n_{\Sigma_y})$  as the  $\pi/2$  counterclockwise rotation of  $\mathbf{t}_\Sigma$ , and  $[z]_x$  stands for the jump of the quantity  $z$  at the point  $x$ .

In Eq. (5) a smooth infinitesimal deformation of the discontinuity  $\Sigma$  is assumed and its normal displacement has been denoted by  $\delta \Sigma$ . This displacement determines another smooth curve  $\Sigma'$  which represents, to first order, the new location of the shock

$$\Sigma' = \{\mathbf{x} + \delta \Sigma(\mathbf{x})\mathbf{n}_\Sigma(\mathbf{x}), \mathbf{x} \in \Sigma\} \quad (6)$$

It is interesting to observe that the fifth and sixth terms in Eq. (5) are divided by  $\mathbf{n}_S \cdot \mathbf{t}_\Sigma$ , which becomes larger when the angle between  $\Sigma$  and  $S$  at  $x = x_b$  is small. Thus, the part of the gradient coming from the shock wave displacement is likely to be more relevant in this case.

The most expensive computations in Eq. (5) (in terms of time and required computational resources) are those which involve the evaluation of  $\delta P$  and  $\delta \Sigma$ . In principle, these can be obtained by solving the linearized flow equations (together with the linearized

<sup>¶</sup>For a plane curve given parametrically as  $f(\eta) = (x(\eta), y(\eta))$ , the curvature is defined as  $\kappa = |(\dot{x}\ddot{y} - \dot{y}\ddot{x})/(\dot{x}^2 + \dot{y}^2)^{3/2}|$ , where the dots denote differentiation with respect to  $\eta$ .

Rankine–Hugoniot conditions) once per each independent deformation (design variable). But, if the design space is large, as is the case in real applications, the computational cost of such a computation is prohibitive. It is then convenient to switch to the control theory approach, which reduces significantly the computational cost of getting the gradients, using the adjoint or dual formulation of the shape design problem.

## II. 2-D Euler Equations and Rankine–Hugoniot Relations

Ideal fluids are governed by the Euler equations [16,17], which express the conservation of mass, momentum (with null viscosity), and energy. In the aeronautical framework, these equations are considered in a domain  $\Omega$  delimited by disconnected boundaries divided into far field  $\Gamma_\infty$  and solid wall boundaries  $S$ . The most common way to pose the Euler equations is in conservative form:

$$\partial_t U + \nabla \cdot \mathbf{F} = 0, \quad \text{in } \Omega \quad (7)$$

where  $U = (\rho, \rho v_x, \rho v_y, \rho E)^T$  are the conservative variables and  $\mathbf{F} = (F_x, F_y)$  is the convective flux vector

$$F_x = \begin{pmatrix} \rho v_x \\ \rho v_x^2 + P \\ \rho v_x v_y \\ \rho v_x H \end{pmatrix}, \quad F_y = \begin{pmatrix} \rho v_y \\ \rho v_x v_y \\ \rho v_y^2 + P \\ \rho v_y H \end{pmatrix} \quad (8)$$

where  $\rho$  is the fluid density,  $\mathbf{v} = (v_x, v_y)$  is the flow velocity in a Cartesian system of reference,  $E$  is the total energy,  $P$  the system pressure, and  $H$  the enthalpy. The system of Eq. (7) must be completed by an equation of state which defines the thermodynamic properties of the fluid. For a perfect gas,

$$P = (\gamma - 1)\rho[E - \frac{1}{2}|\mathbf{v}|^2] \quad (9)$$

where  $\gamma \approx 1.4$  for standard air conditions, and the identity  $\rho H = \rho E + P$  holds.

On the other hand, the Euler equation (7) has to be completed with the following boundary conditions:

$$\mathbf{v} \cdot \mathbf{n}_S = 0, \quad \text{on } S \quad (10)$$

where  $\mathbf{n}_S$  is an inward-pointing unit vector normal to  $S$ , and at the far-field boundary  $\Gamma_\infty$  boundary conditions are specified for incoming waves, whereas outgoing waves are determined by the solution inside the fluid domain [18].

Inviscid flows described by the Euler equations can develop discontinuities (shocks or contact discontinuities) due to the intersection of flow characteristics. When this occurs, the Rankine–Hugoniot conditions relate the flow variables on both sides of the discontinuity. For a shock located at  $\Sigma$ , which propagates with speed  $s$ , these relations are

$$[\mathbf{F} \cdot \mathbf{n}_\Sigma]_\Sigma - s[U]_\Sigma = 0 \quad (11)$$

where  $\mathbf{n}_\Sigma = (n_{\Sigma_x}, n_{\Sigma_y})$  is the unit vector normal to the curve  $\Sigma$  pointing in the same direction as the shock speed  $s$ , and  $[A]_\Sigma$  represents the jump of  $A$  across the discontinuity curve  $\Sigma$ , that is to say,  $[A]_\Sigma = A^+ - A^-$ . For the Euler equations, the Rankine–Hugoniot relations can be written as

$$\begin{cases} [\rho \mathbf{v} \cdot \mathbf{n}_\Sigma]_\Sigma - s[\rho]_\Sigma = 0 \\ [(\rho \mathbf{v} \cdot \mathbf{n}_\Sigma) v_x + P n_{\Sigma_x}]_\Sigma - s[\rho v_x]_\Sigma = 0 \\ [(\rho \mathbf{v} \cdot \mathbf{n}_\Sigma) v_y + P n_{\Sigma_y}]_\Sigma - s[\rho v_y]_\Sigma = 0 \\ [H \rho \mathbf{v} \cdot \mathbf{n}_\Sigma]_\Sigma - s[\rho E]_\Sigma = 0 \end{cases} \quad (12)$$

If a steady problem is considered, the discontinuity velocity vanishes and then Eq. (12) is simplified to

$$\begin{cases} [\rho \mathbf{v} \cdot \mathbf{n}_\Sigma]_\Sigma = 0 \\ [v_x]_\Sigma \rho \mathbf{v} \cdot \mathbf{n}_\Sigma + [P]_\Sigma n_{\Sigma_x} = 0 \\ [v_y]_\Sigma \rho \mathbf{v} \cdot \mathbf{n}_\Sigma + [P]_\Sigma n_{\Sigma_y} = 0 \\ [H]_\Sigma = 0 \end{cases} \quad (13)$$

In this case, along the discontinuity, the following holds [19]:

$$[\rho]_\Sigma \neq 0, \quad [P]_\Sigma \neq 0, \quad [\mathbf{v} \cdot \mathbf{n}_\Sigma]_\Sigma \neq 0, \quad [\mathbf{v} \cdot \mathbf{t}_\Sigma]_\Sigma = 0 \quad (14)$$

## III. Continuous Adjoint Formulation for the Steady Euler Equations

When developing an adjoint method to address optimal design problems in aeronautics, one of the main mathematical difficulties is the presence of discontinuities (shock waves) [8,9,20–22]. This is due, in particular, to the intrinsic complexity of the adjoint system in the presence of shocks. Indeed, in the presence of shock discontinuities, the formal linearization of the state equations, which can be rigorously justified for smooth solutions, fails to be true and the adjoint system changes its nature. Indeed, when this occurs, the state of the system needs to be rather understood as a multibody one in which both the state itself at both sides of the shock and the geometric location of the shock are considered as part of the state.

Thus, the sensitivity of the model needs to take into account both that of perturbations of the solution and that of the location of the shock. The linearized flow equations turn out to be the classical ones on both sides of the shock. But an additional linear transport equation along the shock emerges, which stems from the linearization of the Rankine–Hugoniot conditions. This allows defining the adjoint solution in a unique way.

### A. Analytical Formulation of the Continuous Adjoint Method

The adjoint formulation is applied to an optimization problem defined in Eq. (1), and the objective is to evaluate the variation of the functional (2) under shape changes of the surface  $S$ , where the flow governing equations are the steady Euler equations,

$$\nabla \cdot \mathbf{F} = 0, \quad \text{in } \Omega \quad (15)$$

Assuming a flow discontinuity located along a smooth curve  $\Sigma$  that meets the boundary  $S$  at a point  $x = x_b$  and is parameterized, as mentioned above, in such a way that it begins in  $x_b$ , the variation of the functional  $\delta J$  is given by Eq. (5).  $\delta U$  stands for the infinitesimal deformation of the state to both sides of the discontinuity line and solves the linearized Euler equations, while  $\delta \Sigma$  describes the infinitesimal normal deformation of the discontinuity and it solves a linearization of the Rankine–Hugoniot conditions

$$\begin{cases} \nabla \cdot (\mathbf{A} \delta U) = 0, & \text{in } \Omega \setminus \Sigma \\ \delta \mathbf{v} \cdot \mathbf{n}_S = -\delta S \partial_n \mathbf{v} \cdot \mathbf{n}_S + (\partial_{tg} \delta S) \mathbf{v} \cdot \mathbf{t}_S, & \text{on } S \setminus x_b \\ (8W)_+ = 0, & \text{on } \Gamma_\infty \\ [\mathbf{A}(\delta \Sigma \partial_n U + \delta U)]_\Sigma \cdot \mathbf{n}_\Sigma + [\mathbf{F}]_\Sigma \cdot \delta \mathbf{n}_\Sigma = 0, & \text{on } \Sigma \end{cases} \quad (16)$$

with  $(8W)_+$  representing the incoming characteristics on the far-field boundary which correspond to physical boundary conditions in the Euler problem.  $\partial \mathbf{F} / \partial U = \mathbf{A}$  is the Jacobian matrix,  $\partial_n = \mathbf{n} \cdot \nabla$  and  $\partial_{tg} = \mathbf{t} \cdot \nabla$  are the normal and tangential derivatives, respectively.

Note that system (16) must be solved in two steps: first we find the flow variation  $\delta U$  to both sides of the shock by solving the linearized Euler equations together with the boundary conditions on  $S$  and  $\Gamma_\infty$ . Once  $\delta U$  is known, we use the last equation in Eq. (16) to obtain the displacement of the shock  $\delta \Sigma$ .

In this case,  $\delta S$ , which describes infinitesimal deformations along the normal direction (3), is an input datum to the design problem. In practice,  $\delta S$  has to be directly realized by means of the admissible design variables thus making impossible arbitrary deformations [23]. Therefore, once the continuous analysis has been developed,

allowing arbitrary deformations, a careful numerical interpretation is required to transfer those results to the context of the admissible design variables.

To eliminate  $\delta P$  and  $\delta \Sigma$  from Eq. (5), the adjoint problem is introduced through the Lagrange multipliers  $(\Psi^T; L^T) = (\psi_1, \psi_2, \psi_3, \psi_4; l_1, l_2, l_3, l_4)$ . Generally speaking, the method of Lagrange multipliers facilitates the calculation of the reduced gradient of the multivariate function, the constraints being in this case the linearized Euler equations and Rankine–Hugoniot conditions in Eq. (16). We assume that  $(\Psi^T; L^T)$  satisfies the following adjoint system:

$$\begin{cases} -\mathbf{A}^T \cdot \nabla \Psi = 0, & \text{in } \Omega \setminus \Sigma \\ \boldsymbol{\varphi} \cdot \mathbf{n}_S = \frac{\partial j}{\partial U}, & \text{on } S \setminus x_b \\ \Psi^T(\mathbf{A} \cdot \mathbf{n}_{\Gamma_\infty})_- = 0, & \text{on } \Gamma_\infty \\ [\Psi^T]_\Sigma = 0, & \text{on } \Sigma \\ \partial_{tg} \Psi^T[\mathbf{F} \cdot \mathbf{t}_\Sigma] = 0, & \text{on } \Sigma \\ \Psi^T(x_b)[\mathbf{F} \cdot \mathbf{t}_\Sigma]_{x_b} = \frac{[j]_{x_b}}{n_S \cdot \mathbf{t}_\Sigma}, & \text{at } x_b \\ L = \Psi|_\Sigma, & \text{on } \Sigma \end{cases} \quad (17)$$

where  $\Psi^T(\mathbf{A} \cdot \mathbf{n}_{\Gamma_\infty})_- = 0$  represents the adjoint boundary conditions for the far field that we describe in more detail later.

The first step of the procedure amounts to multiplying the linearized Euler equations and Rankine–Hugoniot conditions in Eq. (16) by  $\Psi$  and  $L$ , respectively. Then, integrating over the part of the domain where the functions are smooth we obtain the following:

$$0 = \int_{\Omega \setminus \Sigma} \Psi^T \nabla \cdot (\mathbf{A} \delta U) d\Omega + \int_{\Sigma} L^T ([\mathbf{A}(\delta \Sigma \partial_n U + \delta U)]_\Sigma \cdot \mathbf{n}_\Sigma + [\mathbf{F}]_\Sigma \cdot \delta \mathbf{n}_\Sigma) ds \quad (18)$$

After integration by parts in the first term of the right-hand side of Eq. (18) and taking into account the first, fourth, and last equations in Eq. (17) we easily obtain

$$0 = \int_{S \setminus x_b} \Psi^T \mathbf{A} \delta U \cdot \mathbf{n}_S ds + \int_{\Gamma_\infty} \Psi^T \mathbf{A} \delta U \cdot \mathbf{n}_{\Gamma_\infty} ds + \int_{\Sigma} \Psi^T [\mathbf{A} \partial_n U]_\Sigma \cdot \mathbf{n}_\Sigma \delta \Sigma ds + \int_{\Sigma} \Psi^T [\mathbf{F}]_\Sigma \cdot \delta \mathbf{n}_\Sigma ds \quad (19)$$

Let us now analyze separately each of the terms of the RHS of Eq. (19) as follows:

1) The first term of Eq. (19) is an integral over the solid surface  $S$ . Substituting the Jacobian matrix by its value and taking into account the second equation in Eq. (17) the integral becomes [6]

$$\begin{aligned} \int_{S \setminus x_b} \Psi^T \mathbf{A} \delta U \cdot \mathbf{n}_S ds &= \int_{S \setminus x_b} (\delta \mathbf{v} \cdot \mathbf{n}_S) \vartheta ds + \int_{S \setminus x_b} (\boldsymbol{\varphi} \cdot \mathbf{n}_S) \delta P ds \\ &= - \int_{S \setminus x_b} ((\partial_n \mathbf{v} \cdot \mathbf{n}_S) \vartheta + \partial_{tg}((\mathbf{v} \cdot \mathbf{t}_S) \vartheta)) \delta S ds + \int_{S \setminus x_b} \frac{\partial j}{\partial P} \delta P ds \end{aligned} \quad (20)$$

where  $\boldsymbol{\varphi} = (\psi_2, \psi_3)$  and  $\vartheta = \rho \psi_1 + \rho \mathbf{v}_S \cdot \boldsymbol{\varphi} + \rho H \psi_4$ . Note that the last term on the RHS of Eq. (20) is precisely one of the terms that we want to eliminate in Eq. (5).

2) The second term of Eq. (19) is an integral over the far-field surface  $\Gamma_\infty$  which vanishes due to the third equation in Eq. (17). In fact, the adjoint boundary conditions are obtained by imposing

$$\Psi^T \tilde{\mathbf{A}} \delta U = 0, \quad \text{on } \Gamma_\infty \quad (21)$$

where  $\tilde{\mathbf{A}} = \mathbf{A} \cdot \mathbf{n}_{\Gamma_\infty}$ . Let us analyze these linearized equations in more detail. The matrix  $\tilde{\mathbf{A}}$  can be diagonalized as  $\tilde{\mathbf{A}} = R \Lambda R^{-1}$ , and we can write Eq. (21) as

$$\Psi^T R \Lambda R^{-1} \delta U = 0 \quad (22)$$

or, in terms of characteristic variables,  $\delta W = R^{-1} \delta U$ :

$$\Psi^T R \Lambda \delta W = 0 \quad (23)$$

Let us decompose the matrix  $\Lambda$  into its positive and negative parts  $\Lambda = \Lambda^+ + \Lambda^-$ , where Dirichlet boundary conditions have been imposed for the characteristic variables corresponding to incoming characteristics, or negative eigenvalues of  $\tilde{\mathbf{A}}$ . Therefore we have

$$R \Lambda^- \delta W = 0 \quad (24)$$

This assertion is only valid if, as in our case, no variations on the far-field boundary are allowed. Using Eq. (24), Eq. (23) reduces to

$$\Psi^T R \Lambda^+ \delta W = 0 \quad (25)$$

where, if we define the characteristic adjoint variables as  $\Phi = R^T \Psi$ , then Eq. (25) is equivalent to  $\Lambda^+ \Phi = 0$ , that is, the characteristic adjoint variables corresponding to positive eigenvalues have to be set to zero. This condition is written in Eq. (17) as

$$\Psi^T (\mathbf{A} \cdot \mathbf{n}_{\Gamma_\infty})_- = 0, \quad \text{on } \Gamma_\infty \quad (26)$$

A good reference about far-field adjoint boundary conditions can be found in [24].

3) We now consider the last two terms on the RHS of Eq. (19), which are integrals over the discontinuity curve  $\Sigma$  that touches the solid surface at the point  $x_b$ . For sufficiently small values of the deformation  $\delta \Sigma$  it is easy to see that

$$\delta \mathbf{n}_\Sigma = -\partial_{tg}(\delta \Sigma) \mathbf{t}_\Sigma$$

Therefore, the last two terms in Eq. (19) read

$$\begin{aligned} &\int_{\Sigma} \Psi^T [\mathbf{A} \partial_n U]_\Sigma \cdot \mathbf{n}_\Sigma \delta \Sigma ds + \int_{\Sigma} \Psi^T [\mathbf{F}]_\Sigma \cdot \mathbf{t}_\Sigma \partial_{tg} \delta \Sigma ds \\ &= \int_{\Sigma} \Psi^T [\partial_n (\mathbf{F} \cdot \mathbf{n}_\Sigma)]_\Sigma \delta \Sigma ds - \int_{\Sigma} \Psi^T [\mathbf{F}]_\Sigma \cdot \mathbf{t}_\Sigma \partial_{tg} \delta \Sigma ds \end{aligned} \quad (27)$$

On the other hand, on  $\Sigma$  we can decompose the divergence operator in the Euler equations into its tangential and normal components as follows:

$$0 = \nabla \cdot \mathbf{F}|_\Sigma = \partial_{tg}(\mathbf{F} \cdot \mathbf{t}_\Sigma) - \kappa_\Sigma \mathbf{F} \cdot \mathbf{n}_\Sigma + \partial_n(\mathbf{F} \cdot \mathbf{n}_\Sigma) \quad (28)$$

where  $\kappa_\Sigma$  is the curvature of  $\Sigma$ . This last identity holds to both sides of the shock  $\Sigma$  and therefore we have

$$\begin{aligned} 0 &= [\partial_{tg}(\mathbf{F} \cdot \mathbf{t}_\Sigma)]_\Sigma - \kappa_\Sigma [\mathbf{F}]_\Sigma \cdot \mathbf{n}_\Sigma + [\partial_n(\mathbf{F} \cdot \mathbf{n}_\Sigma)]_\Sigma \\ &= [\partial_{tg}(\mathbf{F} \cdot \mathbf{t}_\Sigma)]_\Sigma + [\partial_n(\mathbf{F} \cdot \mathbf{n}_\Sigma)]_\Sigma \end{aligned} \quad (29)$$

due to the Rankine–Hugoniot conditions.

From identity (29), the normal derivative in Eq. (27) can be transformed into a tangential derivative and we can write the RHS of Eq. (27) as

$$\begin{aligned} &-\int_{\Sigma} \Psi^T [\partial_{tg}(\mathbf{F} \cdot \mathbf{n}_\Sigma)]_\Sigma \delta \Sigma ds - \int_{\Sigma} \Psi^T [\mathbf{F}]_\Sigma \cdot \mathbf{t}_\Sigma \partial_{tg} \delta \Sigma ds \\ &= -\int_{\Sigma} \Psi^T \partial_{tg}(\delta \Sigma [\mathbf{F} \cdot \mathbf{t}_\Sigma]_\Sigma) ds \\ &= \int_{\Sigma} \partial_{tg} \Psi^T [\mathbf{F} \cdot \mathbf{t}_\Sigma]_\Sigma \delta \Sigma ds + \Psi^T(x_b) [\mathbf{F} \cdot \mathbf{t}_\Sigma]_{x_b} \delta \Sigma(x_b) \\ &= \int_{\Sigma} \partial_{tg} \Psi^T [\mathbf{F} \cdot \mathbf{t}_\Sigma]_\Sigma \delta \Sigma ds + [j]_{x_b} \delta \Sigma(x_b) \end{aligned} \quad (30)$$

where we have used the sixth equation in Eq. (17), for the last identity.

Having analyzed the terms in Eq. (19), this identity can be rewritten as

$$\begin{aligned} & \int_{S \setminus x_b} \frac{\partial j}{\partial P} \delta P \, ds - [j]_{x_b} \delta \Sigma(x_b) \\ &= - \int_{\Sigma} \partial_{tg} \bar{\Psi}^T [\mathbf{F} \cdot \mathbf{t}_{\Sigma}]_{\Sigma} \delta \Sigma \, ds - \Psi^T(x_b) [\mathbf{F} \cdot \mathbf{t}_{\Sigma}]_{x_b} \delta \Sigma(x_b) \\ &+ \int_{S \setminus x_b} ((\partial_n \mathbf{v} \cdot \mathbf{n}_S) \vartheta + \partial_{tg}((\mathbf{v} \cdot \mathbf{t}_S) \vartheta)) \delta S \, ds \end{aligned} \quad (31)$$

This equation will be used to eliminate the linearized variables from the variation of the functional  $J$  defined in Eq. (5) upon identifying the corresponding terms in Eqs. (5) and (31). Thus, Eq. (5) can be written as

$$\begin{aligned} \delta J(S) = & \int_{S \setminus x_b} \left[ \frac{\partial j}{\partial P} \partial_n P + \mathbf{t} \cdot \partial_{tg} \left( \frac{\partial j}{\partial \mathbf{n}_S} \right) - \kappa \left( j + \frac{\partial j}{\partial \mathbf{n}_S} \mathbf{n}_S \right) \right] \delta S \, ds \\ &+ \int_{S \setminus x_b} [(\partial_n \mathbf{v} \cdot \mathbf{n}_S) \vartheta + \partial_{tg}((\mathbf{v} \cdot \mathbf{t}_S) \vartheta)] \delta S \, ds \\ &+ [j(P)]_{x_b} \frac{\mathbf{n}_S \cdot \mathbf{n}_{\Sigma}}{\mathbf{n}_S \cdot \mathbf{t}_{\Sigma}} \delta S(x_b) - \mathbf{t} \cdot \left[ \frac{\partial j}{\partial \mathbf{n}_S} \right]_{x_b} \delta S(x_b) \end{aligned} \quad (32)$$

Using the expressions (17) and (32) we are able to solve any shape design problem with the Euler equations. However, this strategy is difficult to implement in practice because it needs to localize the discontinuity curve  $\Sigma$  to impose the internal boundary conditions on  $\Sigma$  for the adjoint variables, that is, the fourth and fifth equations in Eq. (17). These two equations will be referred to in the sequel as adjoint Rankine–Hugoniot conditions for  $\Psi$ .

Two different methods are proposed for computing the functional gradient using shock information.

1) Method 1: using adjoint Rankine–Hugoniot relations (shock localization).

a) Step 1: Find the discontinuity curve  $\Sigma$  and impose adjoint Rankine–Hugoniot relations over the discontinuity  $\Sigma$  to cancel the dependence of the functional  $J$  with respect to  $\delta \Sigma$ .

b) Step 2: Solve Eq. (17) and evaluate Eq. (32) (or a simplified expression).

2) Method 2: without using adjoint Rankine–Hugoniot relations.

a) Step 1: Ignore the sensitivity of the functional due to the displacement of the discontinuity  $\Sigma$  set as if the flow was continuous across  $\Sigma$ .

b) Step 2: Compute the functional gradient (32) without shock considerations, that is, supposing that  $\delta \Sigma = 0$ . In this case, it is important to note that we are not solving the real adjoint system because the adjoint Rankine–Hugoniot equations are not considered.

c) Step 3: Use the term  $\partial J / \partial \Sigma$  to find a correction for the computed gradient (e.g., introducing design variables in which their main effect is a shock displacement).

### 1. Method 1: Continuous Adjoint System Using Adjoint Rankine–Hugoniot Relations

The direct application of Eqs. (17) and (32) in a real design problem is complex because it is necessary to find the shock curve, the value of the adjoint variables at both sides of the discontinuity, and finally solve the complete adjoint system.

Another possibility consists of assuming normal shock waves [25] (perpendicular to the shock medium's flow direction), and the functional  $j$  as a linear function of  $P$ . In this framework, Eqs. (17) and (32) are simplified to obtain

$$\begin{aligned} \delta J(S) = & \int_{S \setminus x_b} \left[ \frac{\partial j}{\partial P} \partial_n P + \mathbf{t} \cdot \partial_{tg} \left( \frac{\partial j}{\partial \mathbf{n}_S} \right) - \kappa \left( j + \frac{\partial j}{\partial \mathbf{n}_S} \mathbf{n}_S \right) \right] \delta S \, ds \\ &+ \int_{S \setminus x_b} ((\partial_n \mathbf{v} \cdot \mathbf{n}_S) \vartheta + \partial_{tg}((\mathbf{v} \cdot \mathbf{t}_S) \vartheta)) \delta S \, ds \end{aligned} \quad (33)$$

with the following adjoint system:

$$\begin{cases} -\mathbf{A}^T \cdot \nabla \Psi = 0, & \text{in } \Omega \setminus \Sigma \\ \mathbf{t}_{\Sigma} \cdot \partial_{tg} \Psi = 0, & \text{on } \Sigma \\ \Psi \cdot \mathbf{n}_S = \frac{\partial j}{\partial P}, & \text{on } S \\ \Psi^T (\mathbf{A} \cdot \mathbf{n}_{\Gamma_{\infty}})_- = 0, & \text{on } \Gamma_{\infty} \end{cases} \quad (34)$$

To solve the continuous adjoint equations (34) and evaluate Eq. (33) is easier than to use Eq. (17) and evaluate Eq. (32). This is because, in the first case it is not necessary to find the value of the adjoint variables on both sides of the shock (which numerically is a very complex task). The viability of this approach will be shown in Sec. IV.

### 2. Method 2: Continuous Adjoint System Without Using Adjoint Rankine–Hugoniot Relations

The variation of the functional  $J$  in Eq. (32) can be written as

$$\begin{aligned} \delta J(S) = & \int_{S \setminus x_b} G \delta S \, ds + G_{x_b} \delta S(x_b) \\ &+ \int_{\Sigma} G^{\text{shock}} \delta \Sigma \, ds + G_{x_b}^{\text{shock}} \delta \Sigma(x_b) \end{aligned} \quad (35)$$

where  $G$  is the local gradient of  $J$  with respect to an infinitesimal movement of  $S$  in a normal direction  $\mathbf{n}_S$  to the surface  $S$ , and  $G^{\text{shock}}$  is the local gradient of  $J$  with respect to an infinitesimal movement of  $\Sigma$  in a normal direction  $\mathbf{n}_{\Sigma}$  to the discontinuity surface  $\Sigma$ . As before,  $x_b$  denotes the point in which the discontinuity touches the solid surface,

$$\begin{aligned} G = & \frac{\partial j}{\partial P} \partial_n P + \mathbf{t} \cdot \partial_{tg} \left( \frac{\partial j}{\partial \mathbf{n}_S} \right) - \kappa \left( j + \frac{\partial j}{\partial \mathbf{n}_S} \mathbf{n}_S \right) \\ &+ (\partial_n \mathbf{v} \cdot \mathbf{n}_S) \vartheta + \partial_{tg}((\mathbf{v} \cdot \mathbf{t}_S) \vartheta) \end{aligned} \quad (36)$$

$$G_{x_b} = \frac{\partial j}{\partial P} \partial_n P + \mathbf{t} \cdot \partial_{tg} \left( \frac{\partial j}{\partial \mathbf{n}_S} \right) - \kappa \left( j + \frac{\partial j}{\partial \mathbf{n}_S} \mathbf{n}_S \right) + [j(P)]_{x_b} \frac{\mathbf{n}_S \cdot \mathbf{n}_{\Sigma}}{\mathbf{n}_S \cdot \mathbf{t}_{\Sigma}} \quad (37)$$

where in  $G_{x_b}$ , the term  $[j(P)]_{x_b}[(\mathbf{n}_S \cdot \mathbf{n}_{\Sigma}) / (\mathbf{n}_S \cdot \mathbf{t}_{\Sigma})]$ , which depends on the angle between the shock wave and the solid surface, appears. This term can be easily computed by using a finite difference strategy with some selected design variables over the solid surface (with influence over the shock), or by a direct evaluation. Notice that this term is well evaluated when a discrete adjoint strategy or a finite difference method is used.

On the other hand, terms which depend on the shock wave displacement are computed as

$$G^{\text{shock}} = \partial_{tg} \bar{\Psi}^T [\mathbf{F} \cdot \mathbf{t}_{\Sigma}]_{\Sigma} \quad (38)$$

$$G_{x_b}^{\text{shock}} = \Psi^T [\mathbf{F} \cdot \mathbf{t}_{\Sigma}]_{x_b} - \frac{[j(P)]_{x_b}}{\mathbf{n}_S \cdot \mathbf{t}_{\Sigma}} \quad (39)$$

It is noteworthy that the shock displacement sensitivity  $G^{\text{shock}}$  does not appear in the discrete adjoint method because in that method the shock position is not considered as a design variable and only infinitesimal variations of the solid surface  $S$  shape are considered [11].

It is important to remark that there is a very particular deformation of the solid surface (which produces a shock movement) that could imply an important variation of the cost function. Now efforts must be focused in looking to develop a method that introduces this extra information provided by Eq. (38), and there are at least two ways of doing that.

1) Compute the functional gradient without shock considerations. In a second stage, use the term  $\partial J / \partial \Sigma$  for finding a correction to the computed gradient. For example, by an inverse design problem, find the shape  $S$  which produces a shock deformation equivalent to

$\bar{\Psi}^T[\mathbf{F} \cdot \mathbf{t}_\Sigma]_\Sigma$  which is the greatest descent direction using the shock displacement. Finally, use the shape  $S$  which produces a shock deformation as a new surface design variable.

2) Pose the following inverse design problem: find the surface variation that produces only an infinitesimal shock wave displacement over the surface. As before, this shape function which only moves the shock will be used in the optimization problem as a new surface design variable.

## B. Discretization of the Adjoint Equations

We have used a standard edge-based finite volume formulation on the dual grid [26–28], obtained by applying the integral formulation of the adjoint equations to a dual grid control volume  $\Omega_j$  surrounding any given node  $j$  of the grid and performing an exact integration around the outer boundary of this control volume. Using the divergence theorem

$$|\Omega_j| \frac{d\Psi_j}{dt} - \mathbf{A}_j^T \int_{\Gamma_j} \Psi \mathbf{n} dS = |\Omega_j| \frac{d\Psi_j}{dt} - \sum_{k=1}^{m_j} \mathbf{f}_{jk} \cdot \mathbf{n}_{jk} S_{jk} = 0 \quad (40)$$

where  $\mathbf{A}_j^T$  is the (transposed) Euler Jacobian evaluated at the node  $j$ ,  $\Gamma_j$  is the boundary of  $\Omega_j$ , and  $|\Omega_j|$  its area. For every neighbor node  $k$  of  $j$ ,  $\mathbf{n}_{jk}$  is the outward unit vector normal to the face of  $\Gamma_j$  associated with the grid edge connecting  $j$  and  $k$  and  $S_{jk}$  is its length,  $\mathbf{f}_{jk}$  is the numerical flux vector at the said face,  $\Psi_j$  is the value of  $\Psi$  at the node  $j$  (it has been assumed that  $\Psi_j$  is equal to its volume average over  $\Omega_j$ ), and  $m_j$  is the number of neighbors of the node  $j$ . The solution is advanced in time using a multistage Runge–Kutta method. Next, we review several alternative schemes for the computation of the numerical flux vector.

### 1. Central Scheme with Artificial Dissipation

In the current work, we have developed a central scheme inspired by the standard Jameson–Schmidt–Turkel scheme [29], following the adaptation to unstructured flow solvers presented in [30]. In our scheme, the numerical flux is computed as

$$f_{jk}^{\text{cent}} \equiv \mathbf{f}_{jk} \cdot \mathbf{n}_{jk} = A_{jk}^T \left( \frac{\Psi_j + \Psi_k}{2} \right) + d_{jk} \quad (41)$$

where  $A_{jk}^T \equiv \mathbf{A}_j^T \cdot \mathbf{n}_{jk}$  is the projected Jacobian, and  $d_{jk}$  denotes the artificial dissipation. A simplified, fourth order differences scheme has been chosen for the artificial dissipation

$$d_{jk} = \epsilon_{jk}^{(4)} (\nabla^2 \Psi_j - \nabla^2 \Psi_k) \Phi_{jk} \lambda_{jk} \quad (42)$$

where  $\nabla^2$  denotes the undivided Laplacian,  $\epsilon_{jk}^{(4)}$  are user-defined constants, and  $\lambda_{jk}$  is the local spectral radius. Finally  $\Phi_{jk}$  is introduced to account for the stretching of the mesh cells.

### 2. Roe's Upwind Scheme

In addition to the central scheme presented previously, an upwind scheme based upon Roe's flux difference splitting scheme [31,32] has been developed for the adjoint equations.

In our case, the aim is to use an upwind-type formula to evaluate a flow of the form  $\mathbf{A}^T \cdot \nabla \Psi$ . Taking into account that  $\mathbf{A}^T = -(P^T)^{-1} \Lambda P^T$ , where  $\mathbf{A}^T = \mathbf{A}^T \cdot \mathbf{n}$  is the projected Jacobian matrix,  $\Lambda$  is the (diagonal) matrix of eigenvalues and  $P$  is the corresponding eigenvector matrix, the upwind flux is computed as

$$f_{jk}^{\text{upw}} = \frac{1}{2} (A_j^T (\Psi_j + \Psi_k) + (P^T)^{-1} |\Lambda| P^T \delta \Psi) \quad (43)$$

where  $f_{jk}^{\text{upw}} \neq f_{kj}^{\text{upw}}$ .

## IV. Numerical Experiments

The aim of this section is to investigate, with some numerical experiments, the significance of imposing the adjoint Rankine–Hugoniot internal boundary conditions into the functional gradient computation.

The proposed problem consists of minimizing the wave drag using, as initial geometry, a NACA 0012 airfoil. Gradients of the cost function are obtained with respect to variations of 50 Hicks–Henne sine “bump” functions [23], centered at various locations along the upper surfaces of the baseline airfoil. The locations of these geometry perturbations are ordered sequentially such that they start at the 25% of the chord (upper surface) and proceed forward to the trailing edge until the 75% of the chord (upper surface); see Fig. 3 for an example of one-bump functions applied to a NACA 0012 airfoil.

The drag objective function  $C_D$ , on the surface  $S$ , is defined as

$$J_{C_D} = \int_S \frac{P}{0.5 v_\infty^2 \rho_\infty L} \mathbf{n}_S \cdot \mathbf{d} ds, \quad \mathbf{d} = (\cos \alpha, \sin \alpha) \quad (44)$$

where  $\mathbf{n}_S$  is the inward unit vector normal to the boundary  $S$ ,  $\alpha$  is the airfoil angle of attack,  $L$  is the characteristic length of the airfoil, and  $v_\infty$ ,  $\rho_\infty$  are the freestream velocity and density, respectively.

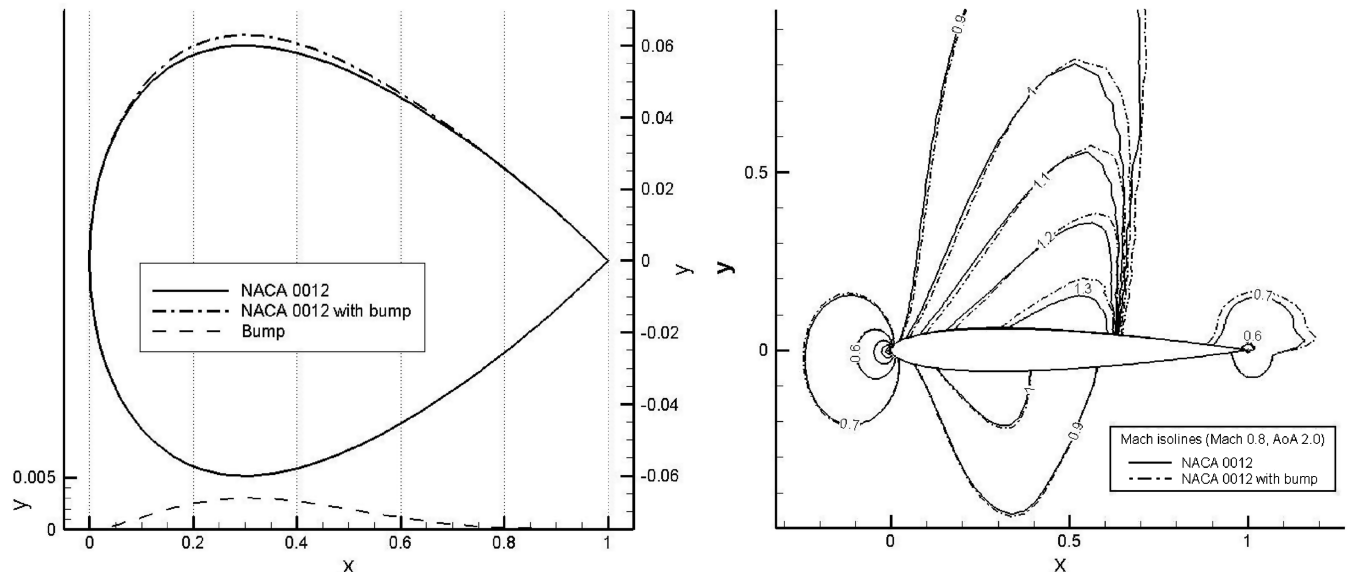


Fig. 3 Geometrical visualization of a Hicks–Henne bump function (left) and the effect produced by this surface perturbation on the Mach distribution (right).

### A. Symmetric Configuration

In this section, a redesign of an airfoil profile NACA 0012 in transonic regime (Mach 0.8,  $\alpha = 0.0$  deg) has been selected as the baseline numerical test. In Fig. 4 the iso-Mach lines (left) and  $C_p$  coefficient (right) of the initial configuration are shown. In this configuration, the shock wave is orthogonal to the NACA 0012 surface and is located on a nearly flat zone (horizontal) of the airfoil profile.

In accordance with the flow results exposed in Fig. 4, we can expect, a priori, that the influence of a shock wave displacement on the  $C_D$  coefficient will be very small because the shock is located on a nearly horizontal plate and the influence of its specific position in this zone on the drag is negligible.

Next, the continuous adjoint formulation developed in this paper is applied. Instead of using the complete adjoint relation over the shock, a simplified version (34) is used. The crucial step of this method is to develop an algorithm for detecting shock waves and subsequently impose the correct adjoint Rankine–Hugoniot relations at the shock location.

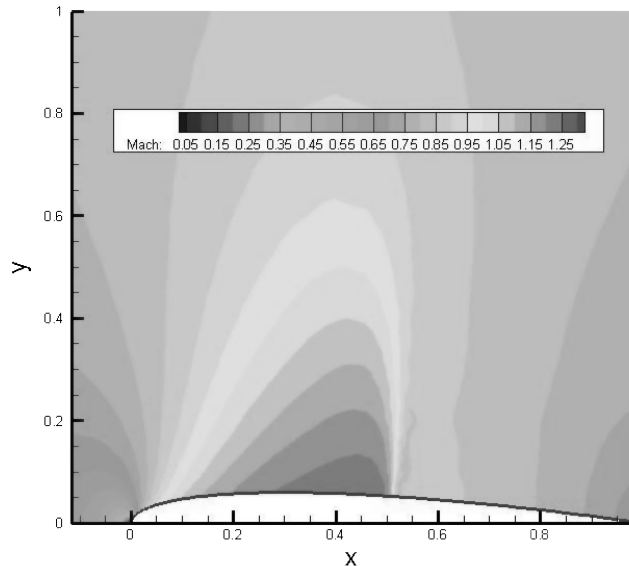


Fig. 4 Iso-Mach lines and  $C_p$  of a NACA 0012 (Mach 0.8,  $\alpha = 0.0$  deg).

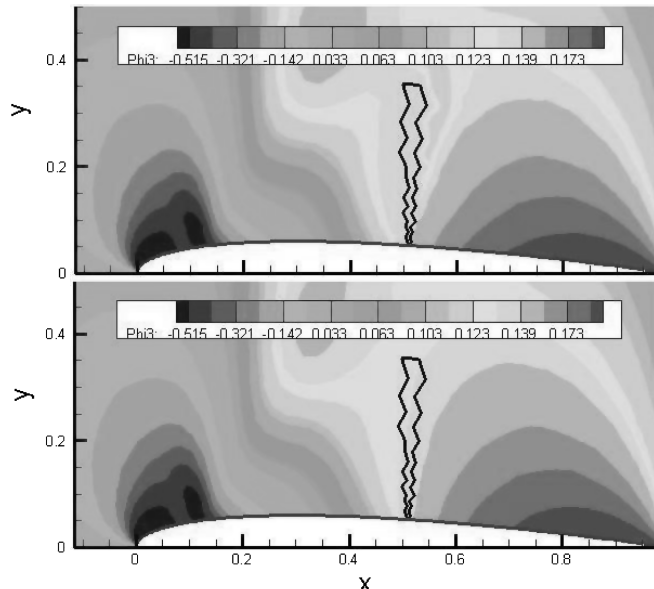


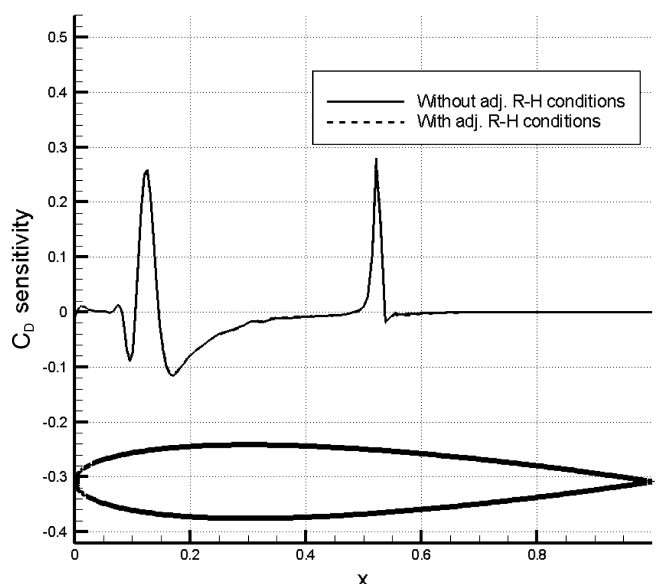
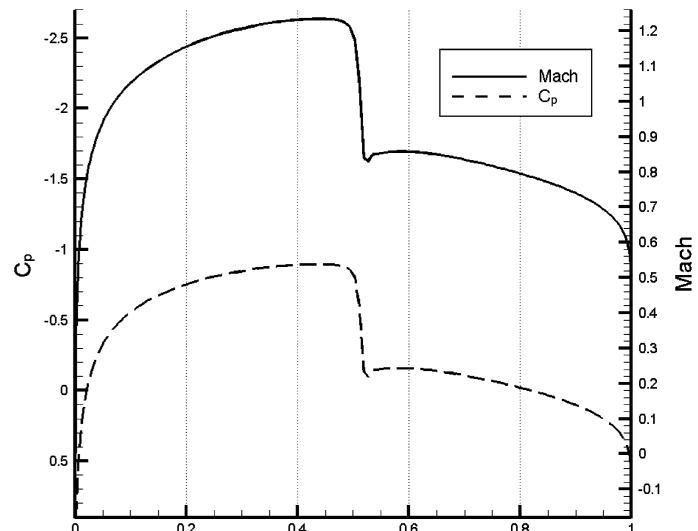
Fig. 5 Symmetric solution: third adjoint variable imposing adjoint Rankine–Hugoniot (R-H) (upper left); third adjoint variable without imposing adjoint R-H (lower left), and drag sensitivity (right).

In Fig. 5 the adjoint variable field (left) is shown (imposing and not imposing the Rankine–Hugoniot relations). On the other hand, a most relevant result is shown in the right part of Fig. 5. In this case the sensitivity of the functional  $C_D$  with respect to infinitesimal variations in the shape of the NACA 0012 is presented (imposing or not, adjoint Rankine–Hugoniot relations on the shock). Results in both cases (with and without Rankine–Hugoniot relations) are almost equal.

To sum up, in this example, internal conditions of Rankine–Hugoniot relations are naturally imposed in the case where the sensitivity of the functional with respect to variations in the position of the shock is negligible. That is to say, the term that multiplies to  $\delta\Sigma$  in Eq. (35) is negligible, and so Eq. (38) vanishes on the shock. This ratifies the fact that under certain circumstances, imposing internal conditions is not necessary.

### B. Asymmetric 2-D Configuration

Now we take a step forward with an asymmetric case. As before, we are looking to redesign an airfoil profile NACA 0012 in transonic



regime but now with an asymmetric flowfield (Mach 0.8,  $\alpha = 1.20$  deg). In Fig. 6 the iso-Mach lines and  $C_p$  are shown. In this case, due to the asymmetry of the configuration, the shock is not perpendicular to the  $x$  axis, so a displacement of the shock produces a significant variation in the functional.

In Fig. 7 (left) both adjoint solutions (with and without using Rankine–Hugoniot relations on the shock) are compared for the third adjoint variable. Also, in Fig. 7 (right) the computed surface gradient in both cases is shown. In contrast to the symmetric case, in this configuration the imposition of the adjoint Rankine–Hugoniot relations has an important influence into the gradient computation.

Figure 8 (left) shows the influence of the shock wave localization in order to impose adjoint Rankine–Hugoniot relations, and the recipe is that the adjoint Rankine–Hugoniot relations must be imposed upwind of the exact shock position. Once the shock wave is located, the adjoint solution is computed (using adjoint Rankine–Hugoniot relations), and the drag surface gradient is evaluated. It is time to integrate the surface drag gradient using 50 Hicks–Henne sine bump functions centered at various locations along the upper surfaces of the baseline airfoil, see Fig. 8 (right).

Finally in Fig. 9 an interesting result is shown. In this case, we are computing the improvement that would provide the correct usage of the adjoint internal conditions in the functional minimization. The validation procedure is as follows:

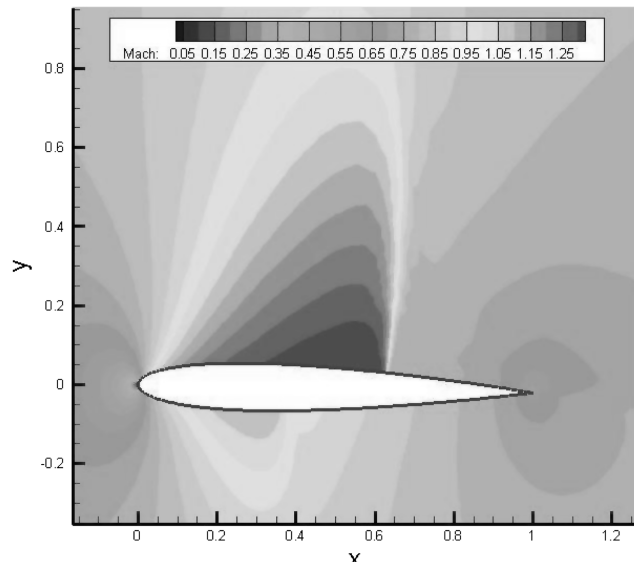


Fig. 6 Iso-Mach lines and  $C_p$  of a NACA 0012 (Mach 0.8,  $\alpha = 1.2$  deg).

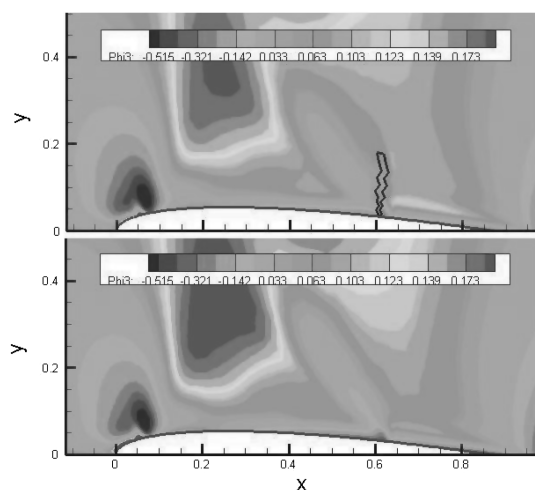
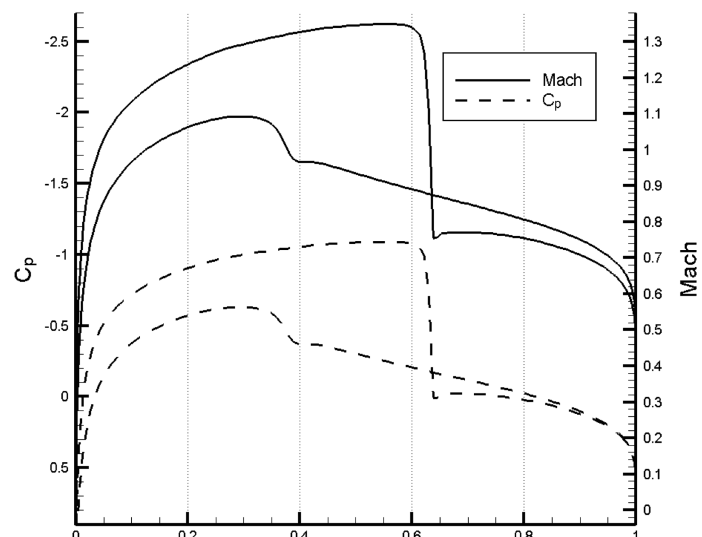


Fig. 7 Asymmetric solution: third adjoint variable imposing adjoint R-H (upper left); third adjoint variable without imposing adjoint R-H (lower left), and drag sensitivity (right).

1) Compute the functional gradients (with and without internal conditions).

2) Normalize the gradient value with respect to the Euclidean norm.

3) Provide a common advance step for both problems (with and without internal conditions).

Using the above procedure, if we do not use the internal conditions drag is reduced to 112 drag counts. On the other hand, if we use the Rankine–Hugoniot adjoint relations we obtain a drag value of 100 drag counts that approximately supposes an improvement in 10% which is remarkable. Still better results are obtained for other functionals that are more sensible to the shock position.

The next step is to state a complete optimization problem to compare the performance between imposing adjoint boundary conditions or not. Figure 10 shows a drag minimization problem.

The goal is to reduce the drag of the NACA 0012 profile, by means of modifications of the surface  $S$ . The angle of attack and Mach number are fixed so that the flow remains transonic (Mach 0.8,  $\alpha = 1.20$  deg). As a constraint we impose that the lift coefficient must be greater than 0.36. In this case, two adjoint problems must be solved: one for computing the drag coefficient sensitivity and the other for computing the lift coefficient sensitivity, and in both cases with and without imposing the adjoint Rankine–Hugoniot conditions. As we can see in this example, to impose the adjoint

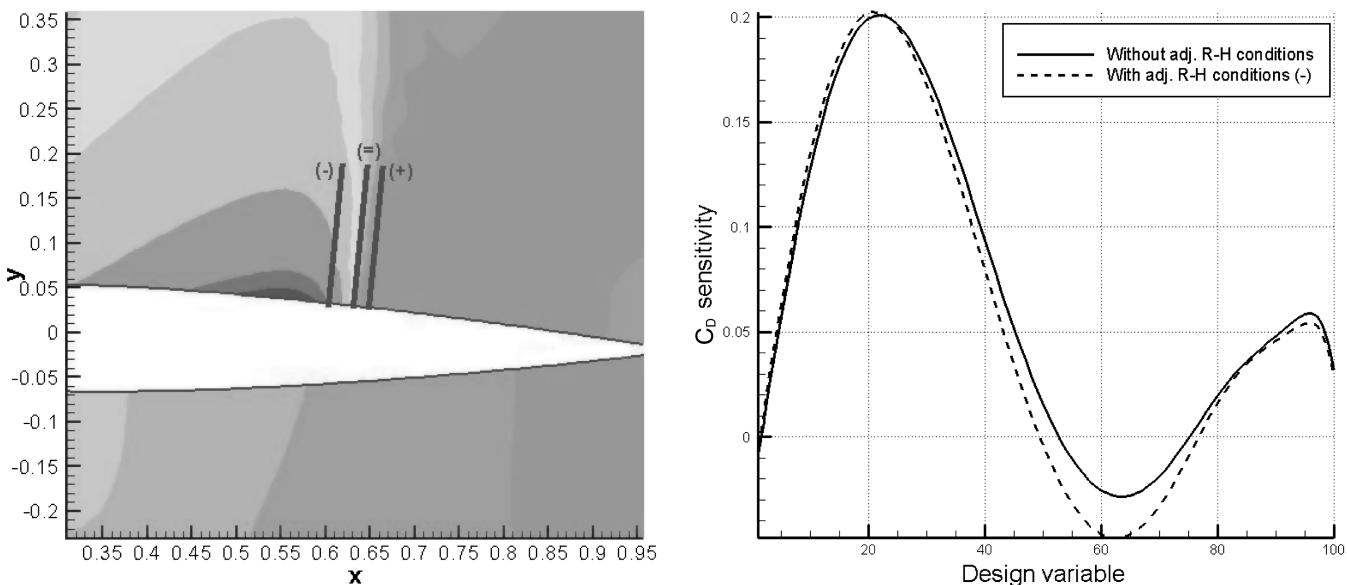


Fig. 8 Shock wave location for imposing adjoint R-H conditions (left) and  $C_D$  gradient (right).

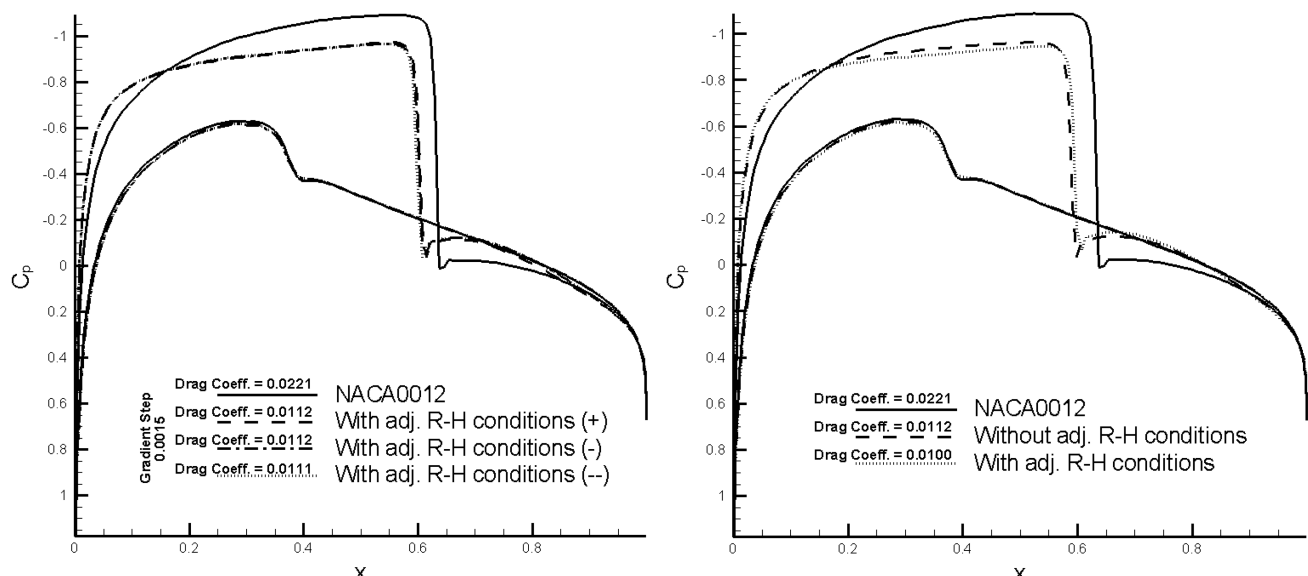


Fig. 9 Estimate improvement using internal boundary conditions.

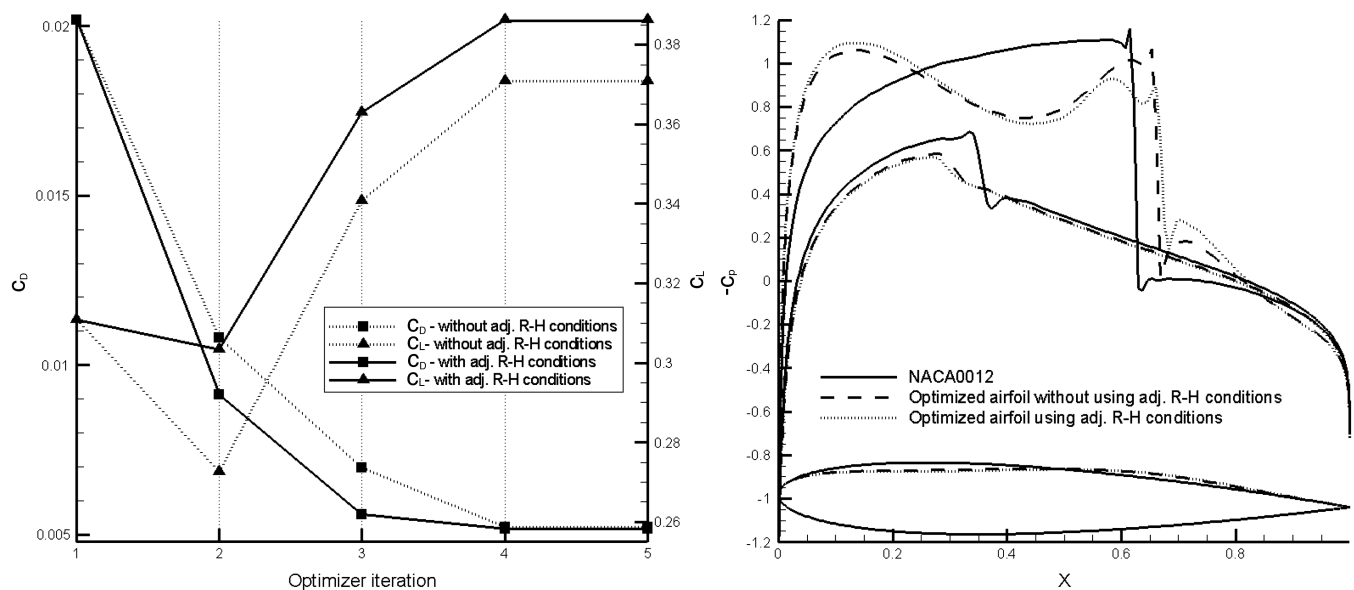


Fig. 10 Complete optimization problem.

internal boundary conditions improves the optimization process in terms of drag minimization and lift maximization.

It is also remarkable that one iteration less is needed to obtain the best result if the adjoint internal boundary conditions are imposed. On the other hand, if the angle of attack would be a design variable of our problem we will expect better optimization results; that is because the obtained lift coefficient is slightly greater than the lower constraint and reducing the angle of attack could improve the drag coefficient (satisfying the lift restriction).

## V. Conclusions

In this work the continuous adjoint methodology for the calculation of gradients of functionals of the flow field defined on the solid surface has been developed taking into account the presence of discontinuities in the flow variables.

The continuous adjoint methodology derives the adjoint problem from the continuous formulation of the flow equations, and as such it constitutes a method that allows one to maintain the rigor throughout the whole procedure. However, it is often necessary to deal with the problem of discontinuities in the solutions of the state equation [11]. In this case, shocks must be treated as singularities where the adjoint Rankine–Hugoniot conditions must be enforced. The enforcement of these conditions is delicate and requires the numerical location of the shock.

Nevertheless, satisfactory results have been obtained without the imposition of these Rankine–Hugoniot conditions across the shock [8,33,34]. On the other hand, in this paper a simplified version of the adjoint Rankine–Hugoniot relations is used and a numerical test revealed the significance of using the functional sensitivity with respect to shock movements. Moreover, some alternative methods are proposed to include extra information that is not provided by the classical finite difference method or the discrete adjoint method, which do not consider the influence of the shock movement.

## Appendix: Variation of the Objective Function in the Presence of Shocks

The purpose of this Appendix is to obtain the following formula:

$$\begin{aligned} \delta J(S) = & \int_S (j'(P)\delta S - j(P)\kappa\delta S + j(P)\partial_n\delta S(x)) ds \\ & - [j(U)]_{x_b} \frac{\delta\Sigma(x_b) - (\mathbf{n}_S \cdot \mathbf{n}_\Sigma)\delta S(x_b)}{(\mathbf{t}_\Sigma \cdot \mathbf{n}_S)} \end{aligned}$$

which has been used in this paper to compute the variation of the objective function when we are dealing with a nonregular flow solution. In fact, the expression above is related to Eq. (5) where, for the sake of simplicity of the proof, it is assumed that  $j = j(P)$ . To proceed with the proof, the variation of  $J(S)$  in the direction  $\delta S\mathbf{n}$  is defined by

$$\delta J(S) = \lim_{\varepsilon \rightarrow 0} \frac{J(S^\varepsilon) - J(S)}{\varepsilon} \quad (A1)$$

where  $S^\varepsilon$  stands for a small deformation of  $S$ , in the normal direction, with the profile  $\delta S$ ,

$$S^\varepsilon = \{x + \varepsilon\delta S\mathbf{n}_S(x), x \in S\}$$

To compute Eq. (A1) we perform an asymptotic expansion of

$$J(S^\varepsilon) = \int_{S^\varepsilon} j(P^\varepsilon) ds \quad (A2)$$

The first step is to change variables in Eq. (A2) to rewrite it as an integral on  $S$ :

$$\begin{aligned} J(S^\varepsilon) &= \int_{S^\varepsilon} j(P^\varepsilon) ds \\ &= \int_S j(P^\varepsilon(x + \varepsilon\delta S\mathbf{n}_S(x))) \text{Jac}(x + \varepsilon\delta S(x)\mathbf{n}_S(x)) ds \\ &= \int_S j(P^\varepsilon(x + \varepsilon\delta S\mathbf{n}_S(x)))(1 - \varepsilon\kappa\delta S(x) + \varepsilon\partial_n\delta S(x)) ds + o(\varepsilon) \end{aligned}$$

where  $\text{Jac}$  is the Jacobian of the transformation, and  $\kappa$  is the curvature of  $S$ .

Now we write an asymptotic expansion for  $j(P^\varepsilon(x + \varepsilon\delta S\mathbf{n}_S(x)))$  with respect to  $\varepsilon$ . If we are far away from the discontinuity  $\Sigma$ , the flow variables are assumed to be smooth and a classical asymptotic expansion holds, namely,

$$j(P^\varepsilon(x + \varepsilon\delta S\mathbf{n}_S(x))) = j(P^\varepsilon(x)) + j'(P^\varepsilon(x))\partial_n P^\varepsilon(x)\varepsilon\delta S(x) + o(\varepsilon) \quad (A3)$$

Moreover, if we also assume that there is a smooth dependence of the flow variables, and, in particular, the pressure  $P^\varepsilon$ , with respect to  $\varepsilon$ , we can write

$$P^\varepsilon(x) = P(x) + \varepsilon\delta P + o(\varepsilon)$$

Thus, the integrand in Eq. (A3) can be written as

$$j(P) + \varepsilon(j'(P)\delta S\mathbf{n}_S(x) - j(P)\kappa\delta S + j(P)\partial_n\delta S(x)) + o(\varepsilon)$$

However, close to the shock wave these asymptotic expansions are no longer valid and we proceed in the following way. We divide  $S$  into two parts  $S = C_1^\varepsilon \cup C_2^\varepsilon$ , where  $C_1^\varepsilon$  is the subset of  $S$  for which the above asymptotics holds. On  $C_1^\varepsilon$  we have

$$\begin{aligned} \int_{C_1^\varepsilon} j(P^\varepsilon(x + \varepsilon\delta S\mathbf{n}_S(x))) ds &= \int_{C_1^\varepsilon} (j(P) + \varepsilon(j'(P)\delta S\mathbf{n}_S(x) \\ &\quad - j(P)\kappa\delta S + j(P)\partial_n\delta S(x)) + o(\varepsilon)) ds \end{aligned}$$

Let us now consider the integral on  $C_2^\varepsilon$ . Let  $x_b \in S \cap \Sigma$ . Note that  $C_2^\varepsilon$  is the neighborhood of  $x_b \in S$  constituted by the points  $x \in S$  such that

$$P(x) = P(x_b^+) + o(\varepsilon) \quad \text{and} \quad P^\varepsilon(x + \delta S\mathbf{n}_S(x)) = P(x_b^-) + o(\varepsilon)$$

where  $P(x_b^+) = \lim_{x \rightarrow x_b} P(x)$  with  $(x - x_b) \cdot t_S > 0$ , and  $P(x_b^+) = \lim_{x \rightarrow x_b} P(x)$  with  $(x - x_b) \cdot t_S < 0$ . In this case

$$\int_{C_2^\varepsilon} j(P^\varepsilon(x + \delta S\mathbf{n}_S(x))) ds = \int_{C_2^\varepsilon} j(P(x_b^-)) ds + o(\varepsilon)$$

whereas

$$\int_{C_2^\varepsilon} j(P(x)) ds = j(P(x_b^+)) \int_{C_2^\varepsilon} ds + o(\varepsilon)$$

To obtain the length of  $C_2^\varepsilon$  we may assume that, at first order, both  $\Sigma$  and  $S$  are straight lines. In this case, it is not difficult to see that this length is given by

$$\frac{\delta\Sigma(x_b) - (\mathbf{n}_S \cdot \mathbf{n}_\Sigma)\delta S(x_b)}{(\mathbf{t}_\Sigma \cdot \mathbf{n}_S)}$$

Therefore we finally obtain

$$\begin{aligned} & \frac{1}{\varepsilon} \left( \int_{S^\varepsilon} j(P^\varepsilon) \, ds - \int_S j(P) \, ds \right) \\ &= \frac{1}{\varepsilon} \left( \int_{C_1^\varepsilon} j(P^\varepsilon(x + \delta S \mathbf{n}_S(x))) \, ds - \int_{C_1^\varepsilon} j(P(x)) \, ds \right) \\ &+ \frac{1}{\varepsilon} \left( \int_{C_2^\varepsilon} j(P^\varepsilon(x + \delta S \mathbf{n}_S(x))) \, ds - \int_{C_2^\varepsilon} j(P(x)) \, ds \right) \\ &= \int_S (j'(P) \delta S - j(P) \kappa \delta S + j(P) \partial_n \delta S(x)) \, ds \\ &- [j(P)]_{x_b} \frac{\delta \Sigma(x_b) - (\mathbf{n}_S \cdot \mathbf{n}_\Sigma) \delta S(x_b)}{(\mathbf{t}_\Sigma \cdot \mathbf{n}_S)} + o(1) \end{aligned}$$

In the general case, that is, when the integrand in Eq. (2) is a function  $j(P, \mathbf{n})$ , the term

$$\int_{S \setminus x_b} j'(P) \delta S$$

must be replaced by

$$\int_{S \setminus x_b} \left( \frac{\partial j}{\partial P} \partial_n P + \frac{\partial j}{\partial \mathbf{n}_S} \cdot \delta \mathbf{n} \right)$$

Taking into account that  $\delta \mathbf{n} = \partial_{tg}(\delta S) \mathbf{t}$  and integrating by parts we easily obtain Eq. (5).

### Acknowledgments

The research described in this paper has been supported under the FuSim-E Programme funded by AIRBUS Spain. Also, this work has been partially supported by Projects MTM2005-00714, MTM2008-03541, and CIT-370200-2007-0022 of the Spanish Ministry of Education and Science (MEC).

### References

- [1] Jameson, A., and Baker, T. J., "Solution of the Euler Equations for Complex Configurations," AIAA Paper 83-1929, 1983.
- [2] Lions, J.-L., *Optimal Control of Systems Governed by Partial Differential Equations*, Springer-Verlag, New York, 1971.
- [3] Pironneau, O., *Optimal Shape Design for Elliptic Systems*, Springer-Verlag, New York, 1984.
- [4] Jameson, A., "Aerodynamic Design via Control Theory," *Journal of Scientific Computing*, Vol. 3, 1988, pp. 233–260.  
doi:10.1007/BF01061285
- [5] Jameson, A., and Kim, S., "Reduction of the Adjoint Gradient Formula in the Continuous Limit," AIAA Paper 2003-0040, 2003.
- [6] Castro, C., Lozano, C., Palacios, F., and Zuazua, E., "A Systematic Continuous Adjoint Approach to Viscous Aerodynamic Design on Unstructured Grids," *AIAA Journal*, Vol. 45, No. 9, Sept. 2007, pp. 2125–2139.  
doi:10.2514/1.24859
- [7] Iollo, A., Salas, M., and Ta'asan, S., "Shape Optimization Governed by the Euler Equations Using an Adjoint Method," Langley Research Center, NASA, TR 191555, Hampton, VA, 1993.
- [8] Giles, M., and Pierce, N., "Analytic Adjoint Solutions for the Quasi One-Dimensional Euler Equations," *Journal of Fluid Mechanics*, Vol. 426, 2001, pp. 327–345.  
doi:10.1017/S0022112000002366
- [9] Matsuzawa, T., and Hafez, M., "Treatment of Shock Waves in Design Optimization via Adjoint Equation Approach," AIAA Paper 98-2537, 1998.
- [10] Cliff, E., Heinkenschloss, M., and Shenoy, A., "Optimal Control for Flows with Discontinuities," *Journal of Optimization Theory and Applications*, Vol. 94, No. 2, Feb. 1997, pp. 273–309.  
doi:10.1023/A:1022616327742
- [11] Castro, C., Palacios, F., and Zuazua, E., "An Alternating Descent Method for the Optimal Control of the Inviscid Burgers Equation in the Presence of Shocks," *Mathematical Models and Methods in Applied Sciences*, Vol. 18, No. 3, 2008, pp. 369–416.  
doi:10.1142/S0218202508002723
- [12] Hicks, R., and Vanderplaats, G., "Application of Numerical Optimization to the Design of Supercritical Airfoils Without Dragcreep," SAE TP 770440, 1977.
- [13] Arian, E., and Salas, M., "Admitting the Inadmissible: Adjoint Formulation for Incomplete Cost Functionals in Aerodynamic Optimization," *AIAA Journal*, Vol. 37, No. 1, 1999, pp. 37–44.  
doi:10.2514/2.690
- [14] Simon, J., "Differentiation with Respect to the Domain in Boundary Value Problems," *Numerical Functional Analysis and Optimization*, Vol. 2, Nos. 7–8, 1981, pp. 649–687.
- [15] Bardos, C., and Pironneau, O., "A Formalism for the Differentiation of Conservation Laws," *Comptes Rendus Mathématique Académie des Sciences, Paris*, Vol. 335, No. 10, 2002, pp. 839–845.  
doi:10.1016/S1631-073X(02)02574-8
- [16] White, F., *Viscous Fluid Flow*, McGraw-Hill, New York, 1974.
- [17] Landau, L., and Lifshitz, E., *Fluid Mechanics*, 2nd ed., Pergamon, Oxford England, U.K., 1993.
- [18] Chakravarthy, S., "Euler Equations—Implicit Schemes and Implicit Boundary Conditions," AIAA Paper 82-0228, 1982.
- [19] Hirsch, C., *Numerical Computation of Internal and External Flows*, Wiley, New York, 1988.
- [20] Giles, M. B., and Pierce, N. A., "Improved Lift and Drag Estimates Using Adjoint Euler Equations," AIAA Paper 99-3293, 1999.
- [21] Majda, A., "The Stability of Multidimensional Shock Fronts," *Memoirs of the American Mathematical Society*, Vol. 41, No. 275, 1983, pp. iv +95.
- [22] Giles, M., *Discrete Adjoint Approximations with Shocks: Hyperbolic Problems: Theory, Numerics, Applications*, Springer-Verlag, Berlin, 2003.
- [23] Hicks, R., and Henne, P., "Wing Design by Numerical Optimization," *Journal of Aircraft*, Vol. 15, 1978, pp. 407–412.  
doi:10.2514/3.58379
- [24] Xie, L., "Gradient-Based Optimum Aerodynamic Design Using Adjoint Method," Ph.D. Thesis, Virginia Polytechnic Institute and State University, Blacksburg, VA, 2002.
- [25] Gadd, G. E., "The Possibility of Normal Shock Waves on a Body with Convex Surfaces in Inviscid Transonic Flow," *Zeitschrift für Angewandte Mathematik und Physik (ZAMP)*, Vol. 11, No. 1, 1960, pp. 51–58.  
doi:10.1007/BF01591802
- [26] Barth, T., and Jespersen, D., "The Design and Application of Upwind Schemes on Unstructured Grids Using Quadratic Reconstruction," AIAA Paper 89-0366, 1990.
- [27] Barth, T., "Aspect of Unstructured Grid and Finite Volume Solvers for the Euler and Navier-Stokes Equations," AIAA Paper 91-0237, 1994.
- [28] Ashford, G., and Powell, K., "An Unstructured Grid Generation and Adaptive Solution Technique for High-Reynolds-Number Compressible Flows," *Computational Fluid Dynamics*, Lecture Series 1996-06, von Karman Institute for Fluid Dynamics, Rhode-Saint-Genèse, Belgium, 1996.
- [29] Jameson, A., Schmidt, W., and Turkel, E., "Numerical Solution of the Euler Equations by Finite Volume Methods Using Runge-Kutta Time Stepping Schemes," AIAA Paper 81-1259, 1981.
- [30] Eliasson, P., *Edge 3.2 Manual*, FOI, 2005.
- [31] Roe, P., "Approximate Riemann Solvers, Parameter Vectors, and Difference Schemes," *Journal of Computational Physics*, Vol. 43, 1981, pp. 357–372.  
doi:10.1016/0021-9991(81)90128-5
- [32] Anderson, W., and Venkatakrishnan, V., "Aerodynamic Design Optimization on Unstructured Grids with a Continuous Adjoint Formulation," AIAA Paper 97-0643, 1997.
- [33] Jameson, A., Sriram, S., and Martinelli, L., "A Continuous Adjoint Method for Unstructured Grids," AIAA Paper 2003-3955, 2003.
- [34] Kim, S., Alonso, J., and Jameson, A., "Design Optimization of High-Lift Configurations Using a Viscous Continuous Adjoint Method," AIAA Paper 2002-0844, 2002.